C h a p t e r 2

Catalytic Cyanide Reduction to Methane and Ammonia at a Mononuclear Fe-site

Adapted from:

Johansen, C. M.; Peters, J. C. *J. Am. Chem. Soc.* **2024**. 146, 5343–5354.

DOI: 10.1021/jacs.3c12395.

2.1 Introduction

Nitrogenases catalyze nitrogen reduction to ammonia (N_2R) as well as the reductive protonation of non-native substrates,[1,2,3,4] including cyanide (CN^-).[5,6,7,8,9,10,11,12,13] These are mechanistically fascinating bio-organometallic transformations which, for the case of CN^- (and CO/CO_2 as well), may involve metal-to-carbon intermediates such as alkyls, carbenes, and carbynes/carbides that are conceptually related to posited intermediates of N_2R (e.g., NNH, NNH_2, NH).

Whereas substantial attention from the synthetic community has been directed towards functional N_2R models with associated mechanistic studies,[14,15,16] there has been only limited attention paid to catalytic cyanide reduction by comparison.[17,18,19,20,21,22] Given potential mechanistic parallels between catalytic N_2 and CN^- reduction, including an isolobal relationship between aminocarbynes (e.g., $M{\equiv}CNR_2$)[23,24,25,26] and their hydrazido ($M{\equiv}NNR_2$) counterparts,[27,28,29] mechanistically well-defined CN^- reduction catalysts present an attractive target for further study. In contrast to terminal hydrazido systems, the reductive protonation of terminal carbynes to liberate products (e.g. CH_4/NH_3) has rarely been observed.[25,30,31,32,33] Indeed, catalytic transformations involving *bona fide* carbyne intermediates, outside of the scope of metathesis reactions,[34,35] are essentially without precedent.

Towards these objectives, our lab reported in 2016 a single-site iron model system capable of mediating the (sub) stoichiometric reductive protonation of CN^- to CH_4 and NH_3.[25] We also characterized a number of species as plausible intermediates of the overall transformation, most notably the carbyne complex $(P_3^{Si})Fe(CNH_2)^+$ (P_3^{Si} represents a tris(phosphino)silyl ligand; Figure 2.1, top).[25] The product distribution observed mimics that of ATP-dependent cyanide reduction by nitrogenases (Figure 2.1, middle), where the major observed products under most conditions studied are methane and ammonia (6 e^- reduction); methylamine (H_3CNH_2; 4 e^- reduction) and methyleneimine ($H_2C{=}NH$; 2 e^- reduction) can also be observed as minor products, along with trace ethane and ethylene.[25,26,27,28]

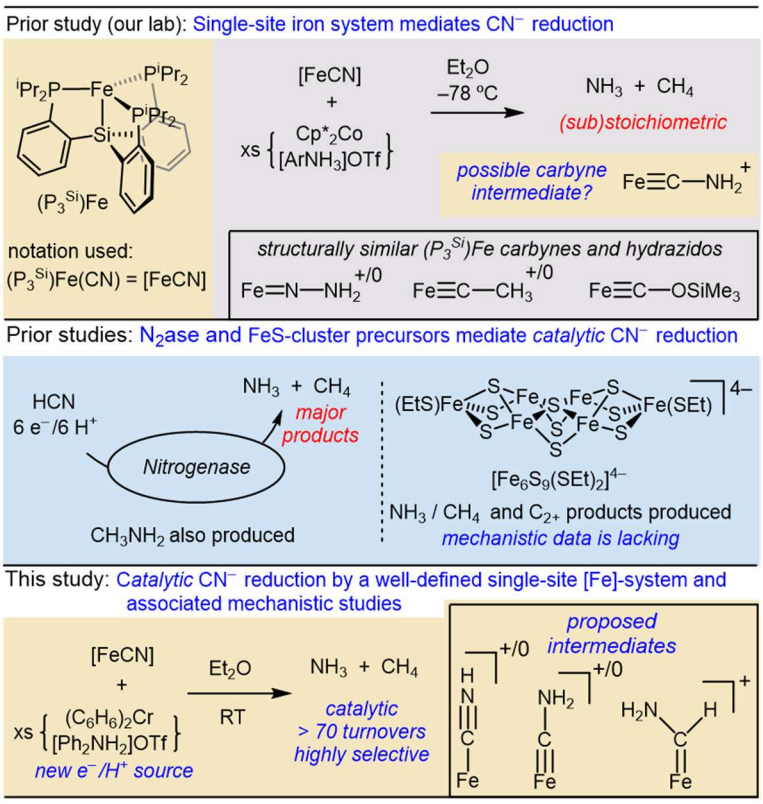

Figure 2.1. Summary of prior studies on stoichiometric and catalytic cyanide reductions mediated by iron complexes as context for this study.[8,22,25,26,44]

Several synthetic Fe–S clusters have also been shown to catalyze cyanide reduction and exhibit substantially higher selectivities for C–C coupled products than has been observed with nitrogenase enzymes as the catalysts (Figure 2.1, middle).[10,11,12,20,21,22] Catalytically relevant species in trans20formations employing such clusters as precatalysts are ill-defined and to date associated mechanistic information has not been forthcoming.

Against this backdrop we have sought conditions for *catalytic* cyanide reduction via our well-defined (P_3^{Si})Fe-system, ideally manifesting product distributions akin to nitrogenases (chiefly favoring the C_1 products CH_4 and CH_3NH_2) and amenable to mechanistic scrutiny. This study presents our findings (Figure 2.1, bottom).

Guided by measured and estimated thermochemical parameters (Figure 2.2A),[36] we show herein that the iron complex (P_3^{Si})Fe(CN) (abbreviated as [FeCN]) efficiently catalyzes cyanide reduction in the presence of acids and reductants. By employing a combination of synthetic, ^{57}Fe Mössbauer, optical, and theoretical studies, we outline a

mechanistic scheme for the catalytic cycle, which can be juxtaposed with that of catalytic nitrogen fixation mediated by analogous iron complexes.

2.2 Results

2.2.1 Canvassing conditions for more efficient [FeCN] reduction

To target the catalytic reduction of CN^- we sought conditions for the proton-coupled reduction of [FeCN] to produce NH_3/CH_4 (or CH_3NH_2) and an [Fe] byproduct that might re-enter a catalytic cycle. In our original report,[25] we described the proton-coupled reduction of [FeCN] using excess [$^{2,5\text{-Cl}}$PhNH$_3$]OTf and Cp*$_2$Co (pK_a 4.5 for [$^{2,5\text{-Cl}}$PhNH$_3$]OTf in THF; all pK_a's reported in THF;[36] $E°$ = −1.9 V for Cp*$_2$Co; all redox potentials are reported in THF and referenced to $Fc^{+/0}$).[37] Such reaction mixtures invariably afforded low yields of NH_3/CH_4 (Figure 2.1A) despite being effective for catalytic N_2R.[38]

Curiously, in our original study we had observed that the cationic aminocarbyne, [FeCNH$_2$]OTf, prepared via double protonation of [FeCN][Na(12-c-4)$_2$],[25] decays upon warming to liberate 0.09 equiv NH_3/Fe and 0.07 CH_4/Fe (Figure 2.2), with [FeCNH]OTf and [FeOTf] as the major Fe-products. This NH_3 yield represents ~50% of that theoretically possible for a disproportionation reaction assuming a stoichiometry of five equivalents of [FeCNH$_2$]OTf providing five H-atom equivalents ([FeCNH$_2$]$^+$→ [FeCNH]$^+$ + H$^+$/e$^-$) to reduce one equivalent [FeCNH$_2$]OTf to NH_3 and CH_4 (Eqn 2.1).

$$6\,[\mathrm{FeCNH_2}] \rightarrow 5[\mathrm{FeCNH}]\mathrm{OTf} + [\mathrm{FeOTf}] + \mathrm{NH_3} + \mathrm{CH_4} \quad \text{(Eqn 2.1)}$$

Based on thermochemical data (Figure 2.2A),[36] removal of a H$^+$/e$^-$ pair from [FeCNH$_2$]$^+$ is equivalent to removal of 1H$^+$/1e$^-$ from an acid/reductant pair with pK_a ~ 7 and $E°$ ~ −1.3 V. Reagents suiting these values would be significantly milder than [$^{2,5\text{-Cl}}$PhNH$_3$]OTf and Cp*$_2$Co. Hence, once [FeCNH$_2$]$^+$ is formed *in situ* via reductive protonation of [FeCN] (pK_a 5.6), comparatively mild reagents should drive net CN^- reduction. Because [FeCN] can be converted to [FeCNH$_2$]OTf with a reductant strength of $E°$ ≈ −1.3 V, we deduced that the 7H$^+$/6e$^-$ reduction of [FeCN] should be accessible with reductants at $E°$ ≈ −1.3 V.

Gratifyingly, stirring [FeCN] with $(C_6H_6)_2Cr$ ($E°$ = −1.2 V, Figure A.23)[39] and $[Ph_2NH_2]OTf$ (pK_a 3.2)[40] in Et_2O at −78 °C and then allowing the reaction mixture to warm to RT overnight yielded 0.75 equiv NH_3/Fe (75% yield per reductant) with [FeOTf] as the major Fe product (Figure 2.2B, and Figure A.9). Moreover, it was established that [FeOTf] reacts cleanly with excess [TBA][CN] to reform [FeCN], setting the stage for catalysis (Figure A.10).

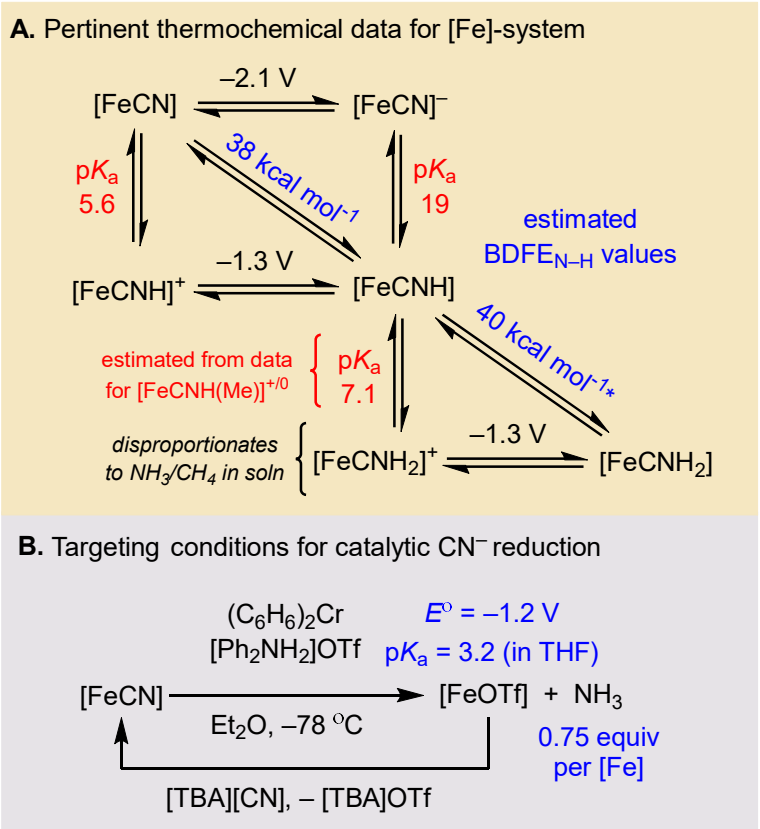

Figure 2.2. Thermochemistry and reagents for stoichiometric [FeCN] reduction. (A) Relevant, previously measured, thermochemical data (values in THF at 25 °C; $E°$ in referenced to $Fc^{+/0}$).[28] (B) Exploring new conditions for reductive protonation of [FeCN].

2.2.2 Catalytic CN^- Reduction

Thus, using [FeCN] (0.72 mM) as a precatalyst, in a reaction mixture containing 140 equiv [TBA][CN] (100 mM), 480 equiv $[Ph_2NH_2]OTf$, and 360 equiv $(C_6H_6)_2Cr$ in Et_2O at 25 °C, yielded 28±5 equiv NH_3/Fe after 80 minutes (Table 2.1, entry 1).

Using these same catalytic conditions, we also analyzed the gaseous products. CH_4 was observed as the major reduced carbon product, with a yield of 25±4 equiv of CH_4/Fe, consistent with a net $7H^+/6e^-$ reduction of CN^- (Eqn 2.2; yield based on consumed $(C_6H_6)_2Cr$ is 47±8%).

$$CN^- + 7\,H^+ + 6\,e^- \rightarrow CH_4 + NH_3 \quad \text{(Eqn 2.2)}$$

Under these conditions trace C_2 products ethylene and ethane were also identified (0.4 equiv C_2H_4 and 0.3 equiv C_2H_6 per Fe). These products correspond to $10H^+/8e^-$ and $12H^+/10e^-$ reductions of CN^-. Combined, these C_2 evolving reactions accounted for less than 2% of the consumed reductant. Hence, the [FeCN] catalyst is nearly quantitatively selective for C_1 products, as is observed via the nitrogenase enzyme.[25,26] H_2 accounts for most of the remaining reducing equivalents (yield based on $(C_6H_6)_2Cr$: 29±11 %). Neither CH_3NH_2 ($4e^-$ product) or CH_2NH ($2e^-$) was detected, regardless of initial temperature, using [FeCN] as a catalyst.

Curiously, whereas synthetic iron catalysts for N_2R have shown highest efficiency at low temperatures due to mitigated HER (Hydrogen evolution reaction) and entropically favored N_2 binding,[41] no such advantage is observed for catalytic cyanide reduction by [FeCN] (entries 2-4). Instead, background HER via combination of this reductant and acid is comparatively slow (*vide infra*). Also, CN^- binds favorably to [Fe(II)] at RT. For reactions started at −78 °C catalytic turnover is slow, reflecting a slow OTf^- for CN^- metathesis step needed to turn the system over (*vide infra*); most of the observed catalysis occurs as the reaction is warmed. For a catalytic reaction run at −20 °C and quenched after 20 minutes, 1.7 equiv NH_3 was detected, demonstrating that catalytic turnover occurs at this temperature, but is relatively slow.

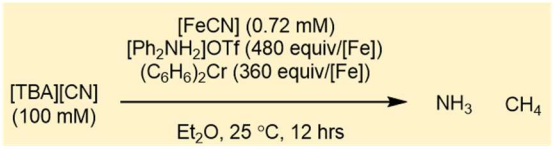

Entry	Change from standard conditions	NH_3 (equiv/Fe)	CH_4 (equiv/Fe)	Yield per reductant (%)[a]
1	None	28±5	25±4	47±8
2	−78 °C → 25 °C	33±6	33±3	55±10
3	−20 °C → 25 °C	35±8	–	58±13
4	0 °C → 25 °C	26±2	–	43±3
5	2.9 mM [FeCN][b]	9.7±0.2	–	65±1
6	0.15 mM [FeCN][b]	73±4	–	24±1
7	No [FeCN][b]	<0.4	<0.3	<1
8	No [TBA][CN][b]	0.7	–	1.2
9	8.0 mM $FeCl_2$ as cat.[b]	0.3	–	5.5
10	8.0 mM $CrCl_2$ as cat.[b]	<0.05	–	<1
11	2.9 mM $(PhBP^{iPr}_3)FeBr$ as cat.[b]	1.4±0.7	1.0±0.1	12±3[c]
12	2.9 mM $(P_3^B)Fe[BAr^F_4]$ as cat.[b]	2.3±0.3	1.6	15.6±0.6
13	Cp_2Co instead of $(C_6H_6)_2Cr$	2.8±0.8	–	12±4
14	Cp^*_2Cr instead of $(C_6H_6)_2Cr$	13.5±3	–	32±6
15	[FeOTf] as cat.	32	–	53
16	Reloaded catalysis[d]	4.1±1.0	–	6.8±1.7

Table 2.1. Results for the catalytic reduction of CN^- to ammonia. (a) Yields assume net 6 e^- reduction to generate NH_3. (b) Catalysis initiated at −78 °C and then allowed to warm gradually to 25 °C (total reaction time of 12 hours). (c) This yield includes 0.6±0.2 equiv CH_3NH_2. (d) After 80 min catalysis under standard conditions (entry 1), soluble Fe species were extracted into Et_2O and then re-exposed to the standard catalytic conditions.

Increasing the catalyst loading to 2.9 mM (entry 5) modestly increased the NH_3 yield relative to reductant present (65±1%). Lowering the catalyst loading (0.15 mM; entry 6) improved the TON for produced NH_3 (73±4 equiv) but led to a corresponding drop in yield per $(C_6H_6)_2Cr$ (24±1%).

A catalyst-free reaction yielded no detectable NH_3, CH_4, or other gaseous carbon products (entry 7). This conclusion is further supported by experiments with [TBA][^{13}CN] as the cyanide source. ^{13}C NMR spectroscopy of catalytic runs using [TBA][^{13}CN] confirmed the formation of $^{13}CH_4$ and consumption of $^{13}CN^-$ (Figures A.5 and A.6). By contrast, a corresponding catalyst-free reaction (under otherwise identical conditions) showed negligible consumption of $^{13}CN^-$ and no observable $^{13}CH_4$. These observations

collectively establish the Fe-catalyst is required for consumption of substrate and responsible for the NH_3 and CH_4 products.

Catalysis run in the absence of [TBA][CN] produced 0.7 equiv NH_3, with [FeC^{15}N] used to demonstrate that this NH_3 arose solely precatalyst reduction and not N_2R (entry 8, Figure A.4).

The nature of the phosphine-ligated iron catalyst appears to be critical. $FeCl_2$ instead of [FeCN] produced only 0.3 equiv NH_3 under the standard conditions (entry 9), and $CrCl_2$ instead of [FeCN] produced no detectable NH_3 (entry 10). The tris(phosphino)iron complexes $(P_3^B)Fe[BAr^F_4]$[16] and $(PhBP^{iPr}_3)FeBr$[42] (P_3^B represents a trisphosphine borane ligand; $PhBP^{iPr}_3$ represents a trisphosphine borate ligand) showed very moderate activity as (pre)catalysts compared to [FeCN] (entries 11-12). Curiously, for $(PhBP^{iPr}_3)FeBr$, a small amount of methylamine, CH_3NH_2 (0.6±0.2), was detected as a product. These iron phosphine precatalysts produce CH_4 as the major hydrocarbon product, but with a lower selectivity. The ratio of C_2/C_1 products produced is 0.16 and 0.11 for $(P_3^B)Fe[BAr^F_4]$ and $(PhBP^{iPr}_3)FeBr$, respectively (Table A.3), compared to 0.02 for [FeCN].

While $(C_6H_6)_2Cr$ is the favored reductant for CN^- reduction, other reductants including Cp_2Co ($E°$ = −1.33 V, Figure A.25; entry 13) and Cp^*_2Cr ($E°$ = −1.47 V, Figure A.27; entry 14) were modestly competent. The low yields for these reductants do not appear to correlate with the reduction potential of the chemical reductant. Instead, we attribute the strong attenuation in yield to enhanced background HER. Accordingly, we find that the rate of reaction of each reductant independently with $[Ph_2NH_2]OTf$ (to produce H_2), as measured by cyclic voltammetry, inversely correlates with the NH_3 TON observed in a catalytic run when CN^- is present under the standard conditions (see appendix, section A.8.2 for details).

To summarize, we have established a highly selective catalytic system for NH_3 and CH_4 production via reductive protonation of CN^-; the choice of catalyst ([FeCN]) and reductant ($(C_6H_6)_2Cr$) are crucial for observing high turnover and significant yields.

2.2.3 Mechanistic studies

Scheme 2.1 provides a working outline for the catalytic CN^- reduction cycle starting from [FeCN], emphasizing early intermediates of the cycle. To guide the following discussion, summary remarks concerning a plausible pathway are as follows: [FeCN] is first protonated (step a) to form independently characterized $[FeCNH]^+$,[25] which is then reduced (to [FeCNH]; step b) and protonated (step c) to afford the independently characterized aminocarbyne, $[FeCNH_2]^+$.[25] $[FeCNH_2]^+$ is in redox equilibrium with $[FeCNH_2]$ in the presence of $(C_6H_6)_2Cr$ (step d). These carbyne intermediates are suggested to be rate contributing to overall CN^- reduction (see below). Along the ET-PT pathway, $[FeCNH_2]$ can be protonated to form a posited carbene intermediate (step e), $[FeC(H)(NH_2)]^+$. This carbene is modeled via independent generation of its methylated analogue, $[FeC(H)(NMe_2)]^+$ via protonation of $[FeCNMe_2]$ (see below). This observation, and computational evidence, each lend support to C–H bond formation to produce $[FeC(H)(NH_2)]^+$ during catalysis. A direct PCET (proton-coupled electron transfer) pathway from $[FeCNH_2]^+$ to $[FeC(H)(NH_2)]^+$ is also plausible (step f). Finally, a series of downstream (as yet undefined), facile reductive protonation steps of $[FeC(H)(NH_2)]^+$ are proposed to release NH_3 and CH_4 along with [FeOTf] (step g); the latter is returned to [FeCN] via metathesis with [TBA][CN], a step (h) that is turnover limiting.

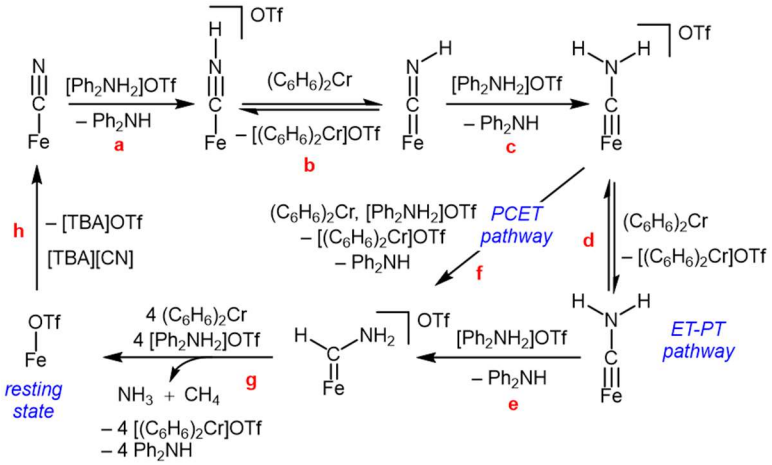

Scheme 2.1. Proposed mechanism for CN^- reduction to NH_3 and CH_4 as catalyzed by [FeCN].

2.2.4 Probing catalyst resting state and deactivation

To probe speciation during catalysis, we prepared [^{57}FeCN] to facilitate monitoring the catalysis by ^{57}Fe Mössbauer spectroscopy via low temperature quenching of catalytic runs initiated at 25 °C. Related studies proved insightful for N_2R catalysis by related Fe systems.[40,43]

Freeze-quenching (77 K) the catalysis after one minute at 25 °C, we found [^{57}FeOTf] as the sole iron-species present (see section S6.2).[44] This result points to [FeOTf] as the catalyst resting state, with metathesis step (h) being turnover limiting. Consistent with this observation, [FeOTf] performs analogous to [FeCN] as a catalyst (Table 1, entry 15). Freeze-quenched snapshots at later reaction times show attenuation in the signal for [^{57}FeOTf] and the growth of unknown iron species. After 80 min, all of the [^{57}FeOTf] has been consumed; the remaining iron species showed poor activity following extraction and (re)subjection to catalytic conditions at 25 °C with fresh acid, reductant and [TBA][CN], yielding only an additional 4.1±1 equiv NH_3 (entry 16). NMR analysis of the post-catalysis mixture revealed evidence of a diamagnetic iron hydride (possibly [Fe(H)($NHPh_2$)]) with the (P_3^{Si})Fe platform intact, as well as free Si(H)P_3 (Figure A.13). Relatedly, iron hydrides (e.g., [Fe(H)(N_2)]) have been shown to be off cycle sinks during catalytic N_2R.[43,45,46]

While our mechanistic studies have focused on the most efficient catalyst, [FeCN], initial studies of the reactivity of (P_3^B)Fe[BAr^F_4] and ($PhBP^{iPr}_3$)FeBr suggest that these less efficient precatalysts are also less stable to excess CN^-. When reacted with 20 equiv [TBA][CN] in Et_2O (in the absence of acid or reductant), free phosphine is observed, indicating partial demetallation as a pathway for deactivation, offering a plausible reason for the lower turnover numbers (Figure A.14 and A.15).

2.2.5 Early N–H Bond Forming Steps

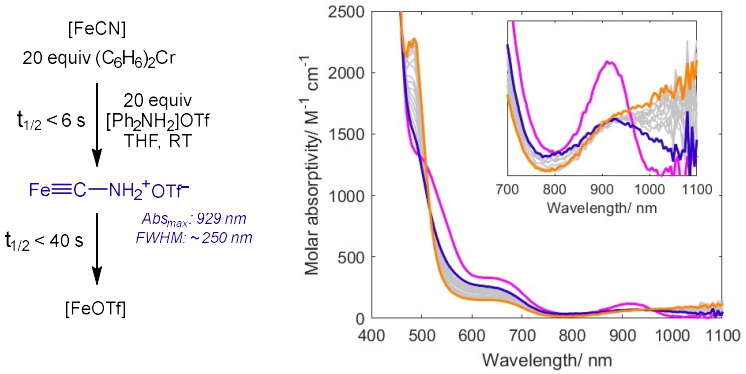

Figure 2.3. UV-vis data showing *in situ* formation of [FeCNH$_2$]OTf (pink trace, 6 s after acid addition) in the reduction of [FeCN] (blue trace) to [FeOTf] (orange trace, 240 s after acid addition).

Since metathesis to produce [FeCN] from [FeOTf] appeared to be turnover limiting we turned to stoichiometric experiments to probe the role/s of early intermediates of reductive protonation in this catalysis.

Exposing a solution containing a mixture of [FeCN] and a large excess (20 equiv) of $(C_6H_6)_2Cr$ (unreactive in the absence of acid) to $[Ph_2NH_2]OTf$ (20 equiv, added via syringe) caused distinct color changes that could be monitored by UV-vis spectroscopy (Figure 2.3). While higher energy absorptions (λ < 600 nm) are complicated by the absorption spectrum of $(C_6H_6)_2Cr^{+/0}$, the lower energy transitions provide a useful handle for the iron speciation. Upon addition of the acid (all 20 equiv) at RT, the characteristic near IR absorption of [FeCN] (λ_{max} = 905 nm, FWHM ≈ 100 nm; blue trace) decayed rapidly ($\tau_{1/2}$ < 6 s) and a new, broader absorbance characteristic of $[FeCNH_2]^+$ (λ_{max} = 929 nm, FWHM ≈ 250 nm; pink trace) was observed.[25] This feature decayed more slowly ($\tau_{1/2}$ ~ 40 s under the conditions studied) with simultaneous growth of a shoulder that extends further into the near-IR, and a strong absorption centered at 485 nm (orange trace). These latter features are consistent with formation of [FeOTf], as was also confirmed by ^{1}H NMR spectroscopy (Figure A.12). Products were also analyzed (1.0 equiv NH_3/Fe and 0.9 equiv CH_4/Fe). These data demonstrate the aminocarbyne $[FeCNH_2]^+$ as an observable on-path intermediate in the conversion of [FeCN] to [FeOTf]. Isosbestic points at 520 nm and 900

nm establish that no further downstream intermediates build-up as $[FeCNH_2]^+$ is converted to [FeOTf] during liberation of NH_3 and CH_4.

To interrogate shorter-lived intermediates, we next studied the consumption of [FeCN] at lower temperature, using fewer equivalents of reductant and acid. Mixing $[^{57}FeCN]$ with $[Ph_2NH_2]BAr^F_4$ and $(C_6H_6)_2Cr$ (2.5 equiv each) in Et_2O at −78 °C for 1 minute, followed by freeze-quench (77 K) and analysis by Mössbauer spectroscopy, showed primarily $[^{57}FeCNH_2]BAr^F_4$ (Figure 2.4A; $\delta = 0.13$ mm s^{-1} and $\Delta E_Q = 1.47$ mm s^{-1}), again supporting the proposed intermediacy of $[FeCNH_2]^+$ during catalysis.[25] These low temperature conditions also allowed identification of the first intermediate of protonation, $[^{57}FeCNH]BAr^F_4$ ($\delta = 0.407$ mm s^{-1} and $\Delta E_Q = 3.20$ mm s^{-1}),[25] as a minor component, consistent with step (a) (Scheme 1).

We also obtained evidence for a facile redox equilibrium between $[FeCNH_2]^{+/0}$ and $(C_6H_6)_2Cr^{+/0}$, as can be expected based on the estimated difference in their reduction potentials ($E°(Fe^{+/0}) \sim -1.2$ V, $E°(Cr^{+/0}) = -1.2$ V; see section S8.3 for data). Relatedly, the available data imply that single electron reduction of $[FeCNH_2]^+$ to $[FeCNH_2]$ (step d) is feasible under conditions relevant to the catalysis. Accordingly, addition of 2.5 equiv $[Ph_2NH_2]BAr^F_4$ to a THF solution of [FeCN] at −80 °C resulted in the immediate formation of $[FeCNH]BAr^F_4$ (Figure 2.4B, blue trace).[25,47] Following this, the solution was titrated with 0-6 equiv $(C_6H_6)_2Cr$ to study its response (Figure 2.4B). During the addition of the 1st equivalent of $(C_6H_6)_2Cr$, UV-vis maxima for $[FeCNH]^+$ (800 nm and 610 nm) decreased in intensity and new maxima appeared reflecting the growth of $[FeCNH_2]^+$ (929 nm and 570 nm; pink trace). Isosbestic points at 570 nm and 860 nm establish no other intermediates build up. Upon addition of further equivalents of $(C_6H_6)_2Cr$, the signals for $[FeCNH_2]^+$ attenuate with corresponding growth of a strong absorbance with a shoulder around 560 nm (orange trace). These changes are consistent with the reduction of $[FeCNH_2]^+$ to $[FeCNH_2]$. Still, even after addition of 6 equiv $(C_6H_6)_2Cr$ a large fraction of $[FeCNH_2]^+$ remained.[48] These results confirm a redox equilibrium between $[FeCNH_2]^{+/0}$ and $(C_6H_6)_2Cr^{+/0}$ (step (d)).

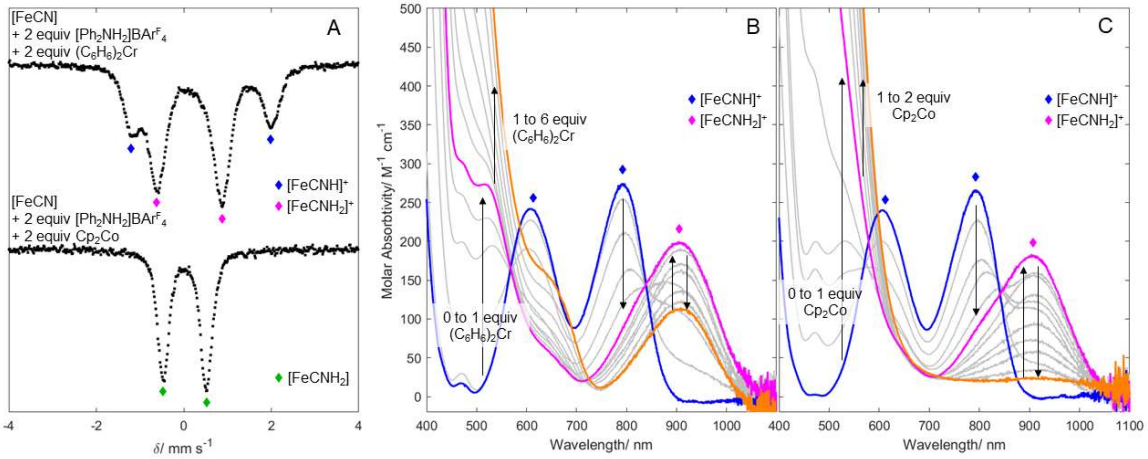

Figure 2.4. Formation of aminocarbynes. (A) ^{57}Fe Mössbauer spectra of reaction of [FeCN] with $[Ph_2NH_2]BAr^F{}_4$ and $(C_6H_6)_2Cr$ or Cp_2Co. (B and C) UV-vis data for reaction of [FeCN] with $[Ph_2NH_2]BAr^F{}_4$ and $(C_6H_6)_2Cr$ (B) or Cp_2Co (C) to form early intermediates $[FeCNH]BAr^F{}_4$ (blue trace), $[FeCNH_2]BAr^F{}_4$ (pink trace) and $[FeCNH_2]^0$ (orange trace).

As expected for such a redox-equilibrium, cobaltocene, a stronger reductant than $(C_6H_6)_2Cr$ ($E°(Cp_2Co^{3+/2+})$ = −1.3 V), completely reduces $[FeCNH_2]^+$ to $[FeCNH_2]$. Accordingly, ^{57}Fe Mössbauer spectra of the reaction between [^{57}FeCN] with $[Ph_2NH_2]BAr^F{}_4$ and Cp_2Co (2.5 equiv each) at −78 °C in Et_2O reveals the formation of a single new species ($\delta = 0.02$ mm s^{-1} and $\Delta E_Q = 0.99$ mm s^{-1}; Figure 2.4A). These parameters closely resemble those of $[FeCNMe_2]$ ($\delta = 0.06$ mm s^{-1} and $\Delta E_Q = 1.12$ mm s^{-1}),[25] consistent with formation of $[FeCNH_2]$. Complete formation of $[FeCNH_2]$ with only 2.5 equivalents of reductant differs markedly from conditions using $(C_6H_6)_2Cr$. Titrations monitored by UV-vis spectroscopy using Cp_2Co still showed $[FeCNH_2]^+$ as an intermediate upon addition of just 1 equiv of Cp_2Co to a mixture of [FeCN] and $[Ph_2NH_2]BAr^F{}_4$ (Figure 2.4C, pink trace). Upon addition of a 2nd equiv of Cp_2Co, $[FeCNH_2]^+$ is fully consumed with concomitant formation of $[FeCNH_2]$ (orange trace).

2.2.6 Evidence for C−H Bond Formation via $Fe=C(H)NH_2^+$

The intermediacy of iron carbynes $[FeCNH_2]^{+/0}$ in catalytic CN^- reduction corresponds to the intermediacy of isolobal hydrazidos $[FeNNH_2]^{+/0/-}$, during Fe-catalyzed

N_2R.[27,28,29,49,50] With this analogy in mind, we wondered whether iron carbynes might be selectivity determining in CN^- reduction, with final N−H bond formation releasing NH_3 (analogous to N_β−H bond formation in N_2R via hydrazido intermediates), resulting in the observed 6 e^- products (CH_4 and NH_3), possibly via a transient carbide [Fe(C)] intermediate. Computational evidence and a study of the reactivity of the methylated carbyne [$FeCNMe_2$] complex instead support C−H bond formation via a carbene intermediate, $[Fe{=}C(H)(NH_2)]^+$, as the next step of the cycle. This path implies that the aminocarbyne is not selectivity determining in the present system; C−N bond cleavage occurs later in the catalytic cycle.

As intermediates downstream of [$FeCNH_2$] cannot be identified during the CN^- reduction process, we studied the reactivity of the more tractable, methylated [$FeCNMe_2$] analogue (Scheme 2). Thus, a reaction between [$FeCNMe_2$] and [Ph_2NH_2]OTf in the absence of added reductant affords a new paramagnetic species, observed via UV-vis and ^{1}H NMR spectroscopy (see SI, section S9); some competing oxidation to $[FeCNMe_2]^+$ (with loss of H_2) is also observed in the reaction mixture, frustrating isolation and purification of the new species. Nonetheless, on the basis of reactivity and ^{57}Fe Mössbauer (*vide infra*), we assign the product of protonation as the aminocarbene $[FeC(H)(NMe_2)]^+$. Its formation is reversible; [$FeCNMe_2$] is cleanly regenerated upon addition of triazabicyclodecene (TBD) base (Scheme 2.2 and Figure A.32).

Scheme 2.2. Protonation and proton-coupled reduction of [FeCNMe$_2$] as a model of [FeCNH$_2$] reactivity.

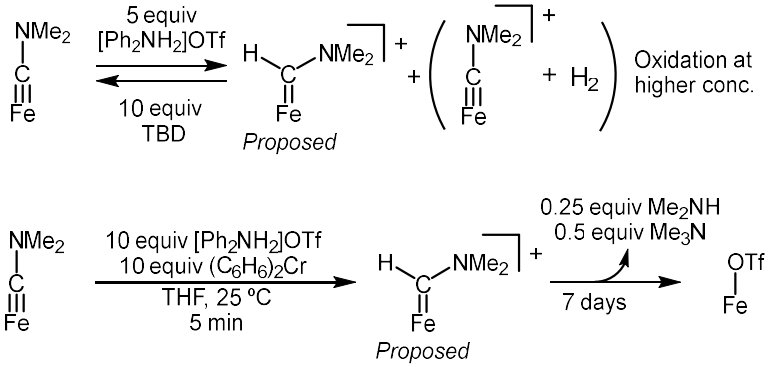

[FeCNMe$_2$] also reacts with 10 equiv [Ph$_2$NH$_2$]OTf in the presence of 10 equiv (C$_6$H$_6$)$_2$Cr in THF at room temperature, and is gradually converted to [FeOTf] over a period 7 days, with Me$_2$NH (0.25 equiv) and (curiously) Me$_3$N (0.5 equiv) detected as the N–containing products.[51] Notably, we had previously observed that [FeCNMe$_2$] is not reduced in combination with Cp*$_2$Co and [$^{2,5\text{-Cl}}$PhNH$_3$]OTf.[25]

While formation of [FeOTf] from [FeCNMe$_2$] is slow in the presence of [Ph$_2$NH$_2$]OTf and (C$_6$H$_6$)$_2$Cr (at 10 equiv each), the [FeCNMe$_2$] is consumed rapidly ($\tau_{1/2}$ ≈ 1 minute at 25 °C) and the same paramagnetic (presumed) carbene species is now also observed as an intermediate. Hence, reacting [FeCNMe$_2$] with excess (C$_6$H$_6$)$_2$Cr and [Ph$_2$NH$_2$]OTf and freeze-quenching the reaction after 5 minutes, revealed a new major species with the parameters δ = 0.40 mm s^{-1} and ΔE_Q =2.25 mm s^{-1} (Figure A.37), consistent with an S = 1 [FeC(H)(NMe$_2$)]$^+$ species with parameters similar to previously characterized S = 1 (P_3^{Si})Fe^{II}–L$^+$ species (L = CO, CNR or N$_2$).[36,52] Taken together these data are highly consistent with [FeC(H)(NMe$_2$)]$^+$ as an intermediate during the reductive protonation of [FeCNMe$_2$] to liberate [FeOTf] and the amine products and suggest [FeC(H)(NH$_2$)]$^+$ would form readily via protonation of [FeCNH$_2$] during CN$^-$ reduction catalysis.

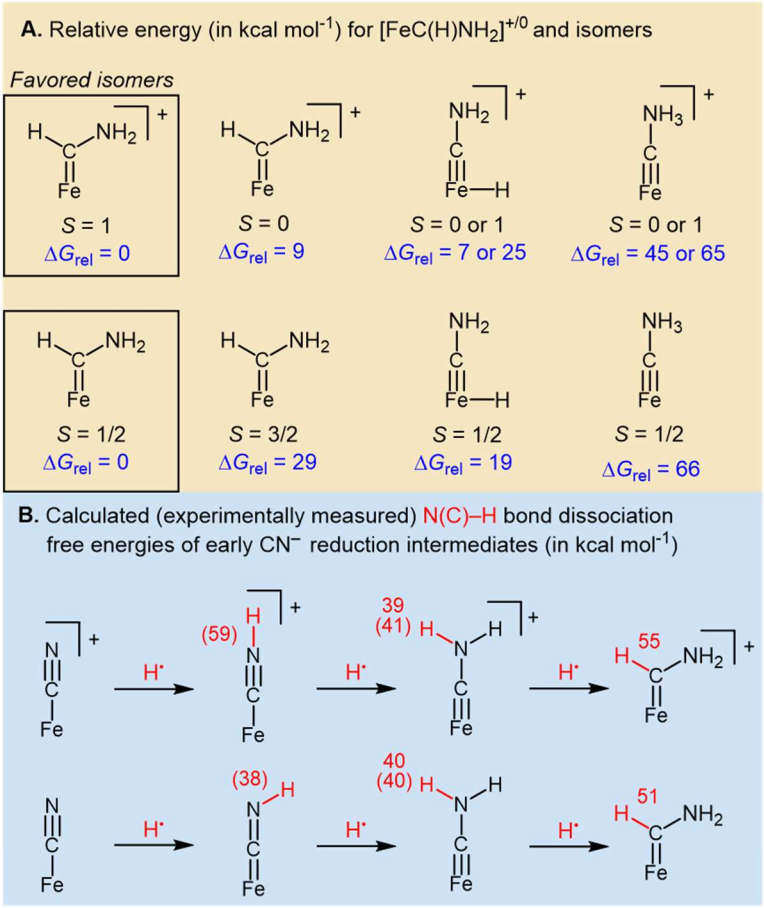

Figure 2.5. Computational study of bond strengths of early N−H bonds (A) Comparing energies of isomers in specified spin states for $[FeC(H)(NH_2)]^{+/0}$. (B) Calculated N−H bond and C–H bond dissociation free energies (BDFE's). Experimentally determined values are provided in parenthesis, for carbynes these are estimated from $[FeCN(H)(Me)]^{+/0}$.[36]

To gain further support for this proposed $[Fe{=}C(H)(NH_2)]^{+}$ intermediate we turned to computational methods to explore the energy of aminocarbene species versus other plausible isomers. The TPSS functional[53] and a def2-TZVP basis set on Fe, with a def2-SVP basis set on all other atoms,[54] reliably replicates experimentally estimated BDFEs for complexes similar to those discussed here.[55] We thus used this approach to compare plausible isomers, with specified spin states, under the addition of H• to the $[FeCNH_2]^{+/0}$ carbynes (Figure 2.5A). We find that iron carbenes $[Fe{=}C(H)(NH_2)]^{+/0}$ in their corresponding $S = 1$ and $S = 1/2$ spin states, respectively, are the lowest energy isomers ($\Delta G_{rel} = 0$ kcal mol^{-1}) when compared to their corresponding ammonium carbyne isomers

($[Fe{\equiv}C{-}NH_3]^{+/0}$; ΔG_{rel} = 45-66 kcal mol^{-1}) and iron carbyne hydrides ($[(H)Fe{\equiv}C{-}NH_2]^{+/0}$; ΔG_{rel} = 7-25 kcal mol^{-1}). Alternative spin states of the iron carbenes (S = 0 or 3/2) are also higher in energy (ΔG_{rel} = 9 and 29 kcal mol^{-1}, respectively). The small ΔG_{rel} of $[(H)Fe{\equiv}C{-}NH_2]^+$ is interesting given that iron hydrides can be catalytic sinks for this system;[46] isomerization between the on-path iron carbene and this iron carbyne hydride might be a relevant deactivation pathway.

The thermodynamic favorability of C−H bond formation (over N−H bond formation) can be rationalized by considering the basicity of the N and C atoms of the iron aminocarbyne. $[FeCNH_2]$ features a planar sp^2-hybridized N atom, suggesting substantial π donation from N, which can be expected to make the N atom less basic than the carbyne C atom. Such a scenario would favor C atom protonation, as observed.

Computationally the carbene $[FeC(H)(NH_2)]^{+/0}$ C−H bonds (51 – 55 kcal mol^{-1}) are much stronger than the carbyne $[FeCNH_2]^{+/0}$ N−H bonds (39-40 kcal mol^{-1}; Figure 2.5B), consistent with the conversion of carbyne to carbene being a thermodynamically favorable step in [FeCN] reduction (Figure 2.6). However, the build-up of $[FeCNH_2]^+$ as an observable intermediate when [FeCN] is reduced to NH_3 and CH_4 (Figure 3), and the slow protonation observed for $[FeCNMe_2]^0$ (Scheme 2.2), suggest a significant kinetic barrier in converting $[FeCNH_2]^{+/0}$ to $[FeC(H)(NH_2)]^{+/0}$ (Figure 2.6). This can be rationalized by a rehybridization at carbon with a corresponding change in spin state upon protonation, which would correlate with a significant kinetic barrier.

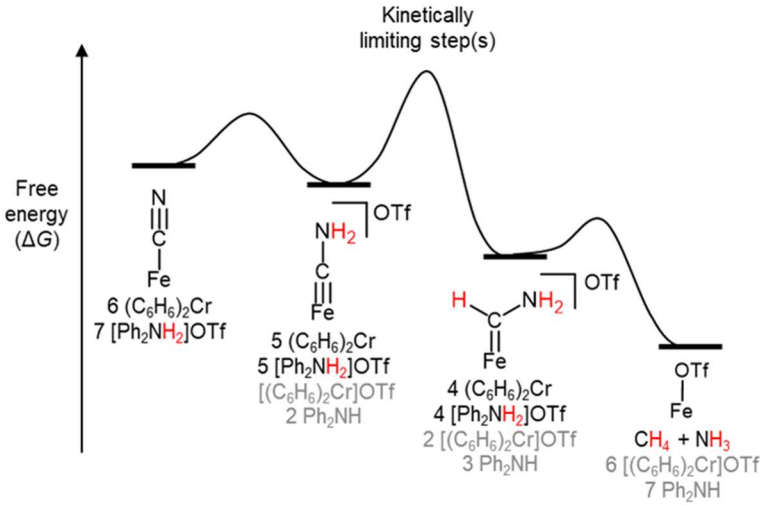

Figure 2.6. Proposed qualitative energy barriers for transformation of [FeCN] to [FeOTf] with key intermediates, $[FeCNH_2]^+$ and $[FeC(H)(NH_2)]^+$ indicated.

2.3 Discussion

2.3.1 Comparison to other Fe-based Catalysts

As introduced above, reported Fe-catalysts for cyanide (or HCN) reduction have exclusively been Fe–S clusters, either as the protein active sites of nitrogenase enzymes,[5,25,26,27,28,13] the extracted cofactors (e.g., FeMoco),[10,11,12] or synthetic clusters.[20,21,22] The extracted cofactors and synthetic clusters studied have been shown to reduce CN^- using weak acids (lutidinium or pH 8 buffered solutions) and lanthanide (II) reductants (SmI_2 or Eu^{II}(DTPA)) as a source of H^+/e^- equivalents. Invariably these systems have produced substantial amounts of C_{2+} products, accounting for 20-40% of the total reduced carbon products, in addition to C_1 products, including CH_4 (and NH_3) or CH_3NH_2.[10,11,12,20,21,22]

By contrast, the [FeCN] catalyst studied herein shows <2% C_{2+} products. Curiously, its reactivity profile more closely resembles that of HCN reduction by MoFe nitrogenase, where C_{2+} products account for <0.1% of the total reduced carbon.[25,26] Still, [FeCN] shows much higher selectivity for the 6 e^- reduction products ($CH_4 + NH_3$) than has been observed for the nitrogenases studied (MoFe and VFe variants), which also show significant CH_3NH_2 production (MoFe, $CH_3NH_2 : CH_4 = 0.39$; VFe, $CH_3NH_2 : CH_4 = 0.66$-1.1).[28] The complex $(PhBP^{iPr}_3)FeBr$, while a less active catalyst system for CN^- reduction (Table 1,

entry 10), more faithfully captures the selectivity of nitrogenases, producing substantial CH_3NH_2 as well as (CH_4 + NH_3). As functional models, the (P_3^B)Fe– and (P_3^{Si})Fe–systems we have studied are distinct in that both have been shown to display catalytic activity for N_2R and CN^- reduction, akin to ATP-dependent nitrogenase enzymes.[1,5,16,43]

2.3.2 Mechanistic findings

The data presented above allow us to posit several important intermediates we believe to be on path for catalytic CN^- reduction by [FeCN] (Scheme 1), and to further consider the observed selectivity. A key observation from low temperature UV-vis titrations includes the finding that [FeCN] is readily protonated by $[Ph_2NH_2]OTf$. The resulting isocyanide $[FeCNH]^+$ can be reduced by $(C_6H_6)_2Cr$, and the resulting $[FeCNH]^0$ product is rapidly protonated to afford the observable aminocarbyne $[FeCNH_2]^+$. With $(C_6H_6)_2Cr$ present as the reductant, $[FeCNH_2]^+$ and $[FeCNH_2]$ have been shown to be in redox equilibrium.

While we observe downstream conversion of $[FeCNH_2]^+$ to [FeOTf] at room temperature (associated with liberation of NH_3 and CH_4), we have been unable to characterize intermediates of this transformation, even at low temperature. However, by reconciling computational data with the observed reactivity of a methylated analogue, $[FeCNMe_2]$, we favor a C–H bond forming step to produce $[FeC(H)(NH_2)]^+$ as the next intermediate from $[FeCNH_2]^+$ along the catalytic pathway (possibly via ET-PT (steps d and e in Scheme 1) or PCET (step f)). This Fischer-type aminocarbene would plausibly be on path for either CH_4 + NH_3 (6 e^-), or CH_3NH_2 (4 e^-), products. The selectivity determining C–N bond cleaving step that produces the 6 e^- products in this system must therefore occur at a later stage of the catalytic cycle, with additional (and facile) $4H^+/4e^-$ transfers (Scheme 1, step g).

From the Fischer carbene (or its one electron reduced congener) several pathways can account for CH_4 and NH_3 products (depicted in Figure 2.7A). Guided by theoretical studies, we can, qualitatively at least, compare them. Ultimately, each specific H^+ and e^- step likely needs to be examined to fully account for CH_4 and NH_3/CH_3NH_2 selectivity, as has been the case for NH_3/N_2H_4 selectivity during N_2R (Figure 2.7B).[28,29,50] However,

acknowledging increased error in theoretical calculations when studying changes in charge state,[56] we have opted to limit our present considerations to the thermodynamics of the addition of a net H-atom to $[FeC(H)_x(NH_2)]^{+/0}$ (x = 1, 2) species, and the associated C−N bond strengths of the ammonium intermediates, $[FeC(H)_x(NH_3)]^{+/0}$, that form. The combined H^+/e^- transfers (Figure 2.7A) are referenced to the combination of $(C_6H_6)_2Cr$ (e^-) and $[Ph_2NH_2]OTf$ (H^+; see appendix A for details).

We consider three pathways in Figure 2.7A (*i*-*iii*) as an expansion on step g introduced in Scheme 1. Pathways *i*-*iii* proceed either via cationic or neutral intermediates and we use +/0 to differentiate between these charge states in the figure.

Starting from the aminocarbene +/0 intermediates, addition of the next H^+/e^- equivalent at N would yield an ammonium carbene, $[FeC(H)(NH_3)]^{+/0}$, which could liberate NH_3 and an iron methylidyne, $[Fe{\equiv}C{-}H]^{+/0}$. The methylidyne is envisioned to be reductively protonated to form CH_4 and [FeOTf] (Figure 2.7A, pathway *i*). The plausibility of iron methylidyne intermediacy in this $P_3^{Si}Fe$ catalyst system is supported by our recent report of the isolation and structural characterization of the methylated analogues $[P_3^{Si}Fe{\equiv}C{-}CH_3]^{+/0}$.[44]

Alternatively, C−H instead of N–H bond formation from $[FeC(H)(NH_2)]^{+/0}$ would yield an iron alkylamine product. We consider computationally such a species as two spin-isomers, a low spin (S = 0, 1/2) η^2-iminium adduct ($[Fe(\eta^2{-}CH_2NH_2)]^{+/0}$) and an intermediate spin (S = 1, 3/2) η^1–alkylamine ($[Fe(\eta^1\text{-}CH_2NH_2)]^{+/0}$). In $[Fe(\eta^1\text{-}CH_2NH_2)]^{+/0}$ intermediates, N−H bond formation is likely kinetically favorable (see below), but from the η^2-iminium adduct we anticipate similar barriers for C−H and N−H bond formation. From either alkylamine isomer, N−H bond formation would yield an alkylammonium product $[FeC(H)_2(NH_3)]^{+/0}$ (pathway *ii*). C−N bond cleavage releases NH_3 and an iron methylidene ($[Fe{=}CH_2]^{+/0}$). While we have not previously characterized a terminal $P_3^{Si}Fe{=}CR_2$ carbene (for R = H or alkyl), cationic, diamagnetic iron methylidenes, $[CpFe(L_2){=}CH_2]^+$ (L = phosphine or CO), have been synthesized by O-atom protonation of a corresponding methoxymethyl iron complex, followed by C−O bond cleavage.[57,58,59]

Such a scenario is akin to the C−N bond cleavage suggested here. Addition of a further $2H^+/2e^-$, releases CH_4 from $[FeCH_2]^{+/0}$.

A CH_3NH_2 selective pathway, $(iii)^{+/0}$ has also been considered, where the addition of H^+/e^- to the C–atom of $[Fe(\eta^2\text{-}CH_2NH_2)]^{+/0}$ results in a methylamine adduct, $[FeNH_2CH_3]^{+/0}$. The latter should readily liberate CH_3NH_2 upon reduction, as has been demonstrated for the ammonia-complex, $[P_3^{Si}FeNH_3]^+$.[60]

Computational analysis of the intermediates along these three pathways shows that C−H bond formation is always thermodynamically favored. Consequently, if the strongest bond is always formed, CN^- reduction would produce CH_3NH_2 instead of CH_4 and NH_3 (Figure 2.7A; pathway *iii*). Hence, to account for the observed CH_4 and NH_3 products, we propose the bulky ^{i}Pr-groups on the P_3^{Si} ligand limit access to the carbyne C-atom and thereby kinetically favor N−H bond formation. This leads to ammonium intermediates $[FeC(H)_x(NH_3)]^{+/0}$ (x = 1,2) that ultimately liberate NH_3 (and then CH_4; Figure 2.7A, pathway *i* and *ii*). This rationalization accommodates the observed mixture of CH_3NH_2 and NH_3 observed when using $(PhBP^{iPr}_3)FeBr$ as a catalyst instead of [Fe] (Table 1, entry 10); the 4-coordinate Fe center in $(PhBP^{iPr}_3)FeBr$ affords a more accessible carbyne intermediate C-atom.[61] Accordingly, the rate of C−H bond formation can compete with N−H bond formation and CH_3NH_2 is an observable product. Relatedly, we suspect that the increased steric bulk at N in $[FeCNMe_2]$ slows the rate of N−H bond formation, leading to the observed product distribution (2:1 Me_3N:Me_2NH).

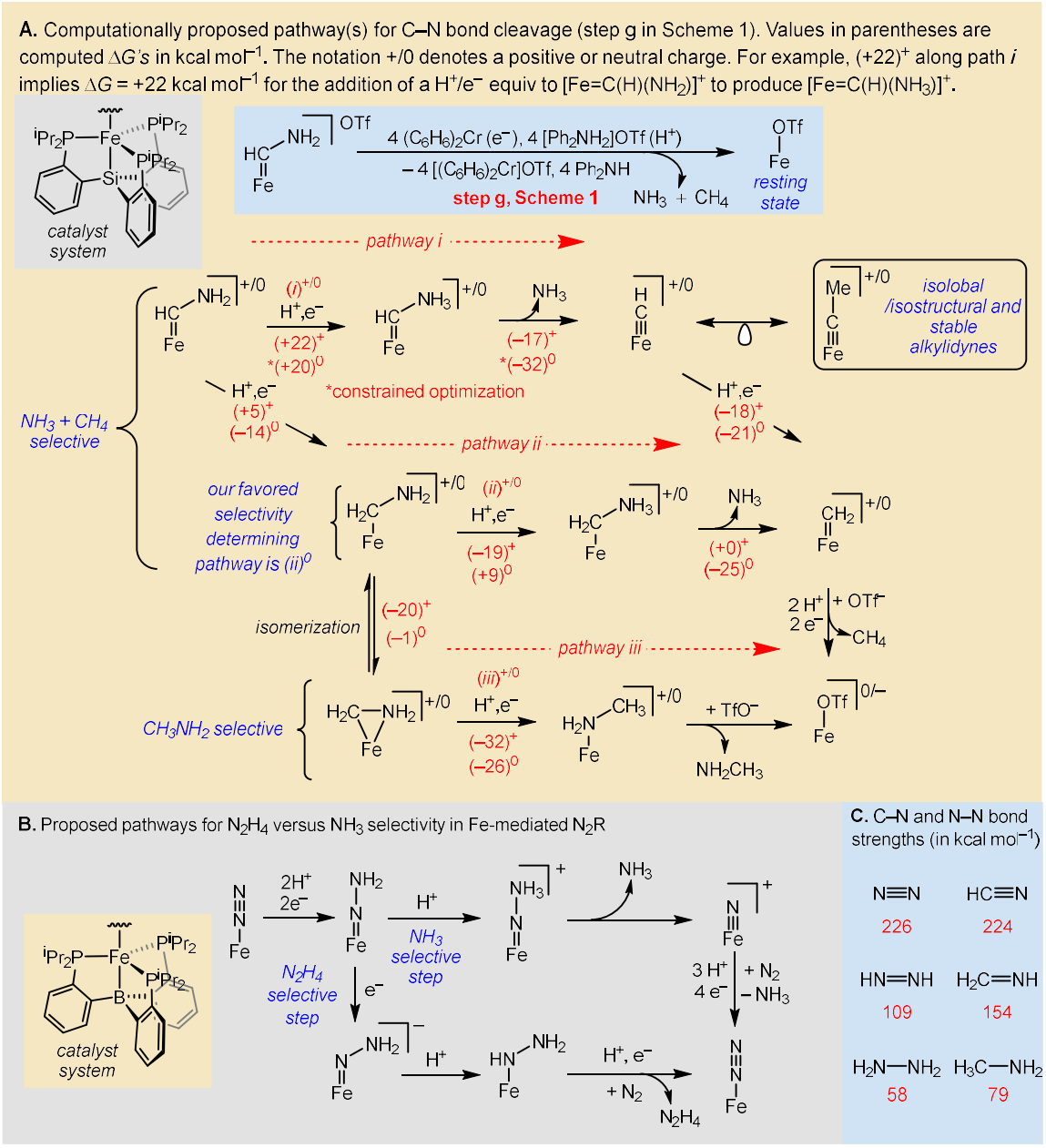

Figure 2.7. Mechanism of C–N bond cleavage and comparison to N–N bond cleavage. (A) Plausible pathways *i* – *iii* for C–N bond cleavage via step g in Scheme 1 for CN^- reduction by the P_3^{Si}Fe-system, attempting to rationalize selectivity, with associated thermodynamic data for stepwise e^-/H^+ transfers en route to product, with values for both cationic (+) and neutral (0) species. Pathway ii^0 is our favored pathway. (B) Comparison with N–N bond cleavage in Fe-mediated N_2R by the P_3^BFe-system, accounting for NH_3 versus N_2H_4 selectivity.[29,50] (C) Comparison of N–N and C–N bond strengths in N_2 and HCN and their further reduced derivatives.[62]

With these considerations, we next compare the NH_3/CH_4 selective pathways (*i* and *ii*). We favor pathway $(ii)^0$ as a pathway involving exothermic and mildly endergonic steps, with C−N bond cleavage occurring from $[FeCH_2NH_3]^0$. Considering pathways $(i)^{+/0}$, they feature highly endergonic N−H bond formation steps (+22 and + 20 kcal mol^{-1}, respectively). As this step is followed by exothermic C−N bond cleavage and reductive protonation of the resulting methylidyne, pathways $(i)^{+/0}$ may nevertheless be kinetically competent.[63] Path $(ii)^+$ features downhill or mildly endergonic steps. We nevertheless disfavor this pathway (compared to $(ii)^0$) due to the high favorability of the diamagnetic $[Fe(\eta^2\text{-}CH_2NH_2)]^+$ (−20 kcal mol^{-1} compared to $[Fe(\eta^1\text{-}CH_2NH_2)]^+$), with subsequent $H^\bullet$ addition at C rather than N being very exothermic from $[Fe(\eta^2\text{-}CH_2NH_2)]^+$.

Our favored path $(ii)^0$ points to a selectivity determining step at the addition of a (net) $H^\bullet$ to $[Fe(\eta^1\text{-}CH_2NH_2)]^0$; the latter constitutes a $4H^+/4e^-$ intermediate of [FeCN] reduction. By contrast, the proposed selectivity determining intermediate during N_2R is $[FeNNH_2]$, a $2H^+/2e^-$ intermediate (Figure 2.7B). Compared to isolobal N≡N, $C{\equiv}N^-$ requires a greater degree of reduction before C−N bond cleavage can occur. This is consistent with the respective C−N and N−N sigma bond strengths: while their triple bond strengths are similar, the bond weakening upon decrease in bond order is much greater for N_2 (Figure 2.7C).[62]

In addition to the high selectivity for CH_4 and NH_3, CN^- reduction of [FeCN] has high C_1 selectivity compared to other Fe-catalysts. When considering the origin of this selectivity, it is worth noting that the addition of multiple cyanide ligands bound to Fe has not been observed during catalysis or chemical experiments. This might be critical for the high selectivity for C_1 products. The precedent for C–C coupling of CO or CNR ligands at mononuclear metal sites requires two of these ligands bound to the metal prior to coupling.[64,65,66,67] The sterically encumbered, four-coordinate $P_3{}^{Si}$-ligand hinders the facile addition of multiple equivalents of CN^-, maintaining the trigonal bipyramidal geometry during catalysis.[68] We propose that this results in the high yields for C_1 products. Accordingly, the more flexible $(P_3{}^B)$Fe-platform[14,55] and the less encumbered $(PhBP^{iPr}{}_3)$Fe-platform[61] both have high C_2/C_1 ratios (0.16 and 0.11, respectively) compared to [FeCN] (0.02). Relatedly,

a previously synthesized and stable compound, $(PhBP^{iPr}_3)Fe(CNR)_2$, demonstrates that $(PhBP^{iPr}_3)Fe$ could accommodate two CN^- ligands (or further protonated derivatives) in a 5-coordinate structure, likely needed for C_2 product formation.[69]

Finally, it is interesting to compare the strength of the reductant used herein for the CN^- reduction ($(C_6H_6)_2Cr$; E °= −1.2 V), with a common reductant used for N_2R via related iron catalysts Cp^*_2Co (E° = −1.9 V). Proposed pathways for catalysis require a turnover limiting potential (E° ≈ −2.0 V) that generates an FeN_2^- species before protonation (to generate FeN_2H) can occur, necessitating reductants as strong as Cp^*_2Co.[38,40,70]

By contrast, the basicity of the CN^- ligand enables protonation of [FeCN] prior to an ET step.[25,36] Consequently, the turnover limiting potential is that of $[FeCNH]^{+/0}$ ($E(Fe^{II/I})$ = –1.3 V), not $[FeCN]^{0/-}$ ($E(Fe^{II/I})$ = –2.1 V), allowing the use of a comparatively mild reductant like $(C_6H_6)_2Cr$. If initial protonation, or PCET, occurs before any independent ET steps, the turnover limiting potential for catalysis can be significantly less reducing. Indeed, Schrock's original triamidoamine Mo-N_2 catalyst system is thought to proceed via an initial PT step, and it is compatible with correspondingly milder reductants (e.g., Cp^*_2Cr) for turnover.[15,71,72]

2.4 Conclusions

In conclusion, we have described the catalytic reductive protonation of CN^- to primarily NH_3 and CH_4, by a mononuclear Fe-complex, with selectivities comparable to those observed for CN^- reduction by nitrogenase. We also report mechanistic studies that show terminal iron aminocarbynes ($FeCNH_2$) intermediates, which are structurally similar to iron hydrazido intermediates ($FeNNH_2$) of Fe-mediated N_2R, as on-path in the CN^- reduction cycle. Experimental and computational studies suggest that these aminocarbynes undergo further C−H bond formation(s) prior to C−N bond cleavage, resulting in the selectivity observed, in contrast to iron hydrazidos during N_2R. Via this study, a terminal transition metal carbyne is hence invoked as a critical intermediate in the catalytic reductive protonation of a robust small molecule (CN^-).

2.5 Cited References

1. Seefeldt, L. C.; Yang, Z.-Y.; Lukoyanov, D. A.; Harris, D. F.; Dean, D. R.; Raugei, S.; Hoffman, B. M. *Chem. Rev.* **2020**. 120, 5082–5106.
2. Seefeldt, L. C.; Rasche, M. E.; Ensign, S. A. *Biochemistry* **1995**. 34, 5382–5389.
3. Lee, C. C.; Hu, Y.; Ribbe, M. W. *Science* **2010**. 329, 642–642.
4. Spatzal, T.; Perez, K. A.; Einsle, O.; Howard, J. B.; Rees, D. C. *Science* **2014**. 345, 1620–1623.
5. Hardy, R. W. F.; Knight, E. *Biochim. Biophys. Acta BBA - Enzymol.* **1967**. 139, 69–90.
6. Kelly, M.; Postgate, J. R.; Richards, R. L. *Biochem. J.* **1967**. 102, 1-3C.
7. Li, J.; Burgess, B. K.; Corbin, J. L. *Biochemistry* **1982**. 21, 4393–4402.
8. Lowe, D. J.; Fisher, K.; Thorneley, R. N. F.; Vaughn, S. A.; Burgess, B. K. *Biochemistry* **1989**. 28, 8460–8466.
9. Fisher, K.; Dilworth, M. J.; Newton, W. E. *Biochemistry* **2006**. 45, 4190–4198.
10. Lee, C. C.; Hu, Y.; Ribbe, M. W. *Angew. Chem. Int. Ed Engl.* **2012**. 51, 1947–1949.
11. Lee, C. C.; Hu, Y.; Ribbe, M. W. *Angew. Chem. Int. Ed Engl.* **2015**. 54, 1219–1222.
12. Lee, C. C.; Hu, Y.; Ribbe, M. W. *Proc. Natl. Acad. Sci.* **2012**. 109, 6922–6926.
13. Roth, L. E.; Tezcan, F. A. *J. Am. Chem. Soc.* **2012**. 134, 8416–8419.
14. Chalkley, M. J.; Drover, M. W.; Peters, J. C. *Chem. Rev.* **2020**. 120, 5582–5636.
15. Yandulov, D. V.; Schrock, R. R. *Science* **2003**. 301, 76–78.
16. Anderson, J. S.; Rittle, J.; Peters, J. C. *Nature* **2013**. 501, 84–87.
17. L. Hughes, D.; Y. Mohammed, M.; J. Pickett, C. *J. Chem. Soc. Chem. Commun.* **1989**. 18, 1399–1400.
18. Pombeiro, A. J. L.; Richards, R. L. *Coord. Chem. Rev.* **1990**. 104, 13–38.
19. Pombeiro, A. J. L.; Guedes da Silva, M. F. C.; Michelin, R. A. *Coord. Chem. Rev.* **2001**. 218, 43–74.

20. Tanifuji, K.; Sickerman, N.; Lee, C. C.; Nagasawa, T.; Miyazaki, K.; Ohki, Y.; Tatsumi, K.; Hu, Y.; Ribbe, M. W. *Angew. Chem. Int. Ed.* **2016**. 55, 15633–15636.
21. Sickerman, N. S.; Tanifuji, K.; Lee, C. C.; Ohki, Y.; Tatsumi, K.; Ribbe, M. W.; Hu, Y. *J. Am. Chem. Soc.* **2017**. 139, 603–606.
22. Tanifuji, K.; Lee, C. C.; Ohki, Y.; Tatsumi, K.; Hu, Y. L.; Ribbe, M. W. *Angew. Chem.-Int. Ed.* **2015**. 54, 14022–14025.
23. Fischer, E. O.; Schneider, J.; Neugebauer, D. *Angew. Chem. Int. Ed. Engl.* **1984**. 23, 820–821.
24. Mokhtarzadeh, C. C.; Moore, C. E.; Rheingold, A. L.; Figueroa, J. S. *Angew. Chem. Int. Ed.* **2017**. 56, 10894–10899.
25. Rittle, J.; Peters, J. C. *Angew. Chem.-Int. Ed.* **2016**. 55, 12262–12265.
26. Lee, Y.; Peters, J. C. *J. Am. Chem. Soc.* **2011**, 133, 4438–4446.
27. Anderson, J. S.; Cutsail, G. E.; Rittle, J.; Connor, B. A.; Gunderson, W. A.; Zhang, L.; Hoffman, B. M.; Peters, J. C. *J. Am. Chem. Soc.* **2015**. 137, 7803–7809.
28. Rittle, J.; Peters, J. C. *J. Am. Chem. Soc.* **2016**. 138, 4243–4248.
29. Thompson, N. B.; Green, M. T.; Peters, J. C. *J. Am. Chem. Soc.* **2017**. 139, 15312–15315.
30. Pombeiro, A. J. L.; Richards, R. L. *Transit. Met. Chem*. **1980**. 5, 281–284.
31. Carvalho, M. F. N. N.; Pombeiro, A. J. L.; Schubert, U.; Orama, O.; Pickett, C. J.; Richards, R. L. *J. Chem. Soc. Dalton Trans.* **1985**. 10, 2079–2084.
32. For an example of protonation and substrate release from a bridging carbyne see: Whitmire, K.; Shriver, D. F. *J. Am. Chem. Soc.* **1980**. 102, 1456–1457.
33. Holt, E. M.; Whitmire, K. H.; Shriver, D. F. *J. Organomet. Chem.* **1981**. 213, 125–137.
34. Wengrovius, J. H.; Sancho, J.; Schrock, R. R. *J. Am. Chem. Soc.* **1981**. 103, 3932–3934.
35. Fürstner, A. *J. Am. Chem. Soc.* **2021**. 143, 15538–15555.

36. Rittle, J.; Peters, J. C. *J. Am. Chem. Soc.* **2017**. 139, 3161–3170.
37. Chalkley, M. J.; Oyala, P. H.; Peters, J. C. *J. Am. Chem. Soc.* **2019**. 141, 4721–4729.
38. Chalkley, M. J.; Del Castillo, T. J.; Matson, B. D.; Peters, J. C. *J. Am. Chem. Soc.* **2018**. 140, 6122–6129.
39. Connelly, N. G.; Geiger, W. E. *Chem. Rev.* **1996**. 96, 877–910.
40. Chalkley, M. J.; Del Castillo, T. J.; Matson, B. D.; Roddy, J. P.; Peters, J. C. *ACS Cent. Sci.* **2017**. 3, 217–223.
41. Ung, G.; Peters, J. C. *Angew. Chem. Int. Ed.* **2015**. 54, 532–535.
42. Betley, T. A.; Peters, J. C. *J. Am. Chem. Soc.* **2003**. 125, 10782–10783.
43. Del Castillo, T. J.; Thompson, N. B.; Peters, J. C. *J. Am. Chem. Soc.* **2016**. 138, 5341–5350.
44. Citek, C.; Oyala, P. H.; Peters, J. C. *J. Am. Chem. Soc.* **2019**. 141, 15211–15221.
45. Buscagan, T. M.; Oyala, P. H.; Peters, J. C. *Angew. Chem. Int. Ed.* **2017**. 56, 6921–6926.
46. Creutz, S. E.; Peters, J. C. *Chem. Sci.* **2017**. 8, 2321–2328.
47. The protonation of [FeCN] to [FeCNH][BAr^F_4] was monitored by observing the shift in the UV-visible spectra maxima at 910 and 540 nm to 790 and 610 nm upon addition of the acid, see Appendix A.
48. Addition of more equivalents $(C_6H_6)_2Cr$ was not possible due to solubility limitations interfering with the UV-vis measurements.
49. Garrido-Barros, P.; Chalkley, M. J.; Peters, J. C. *Angew. Chem. Int. Ed.* **2023**. 62, e202216693..
50. Boyd, E.A.; Peters, J.C. *J. Am. Chem. Soc.* **2023**. 145, 14784–14792.
51. The observation of substantial amounts of Me_3N is perhaps unexpected given the selectivity for NH_3 + CH_4 in the catalytic cyanide reduction reaction. We note that while [$FeCNMe_2$] and [$FeCNH_2$]$^{+/0}$ react with a combination of $(C_6H_6)_2Cr$/Ph_2NH_2]OTf at similar rates, the proposed intermediate [$FeC(H)NMe_2$]$^+$

is consumed much more slowly. This could suggest an alternative reaction pathway, such as bimolecular Me• transfer.

52. L represents a 2 e^- ligand (e.g., carbene, CO, CNMe, N_2). Relevant Mössbauer data for other S = 1 species, where $(P_3^{Si})Fe^{II}–L^+$ represents the cationic species $(P_3^{Si})Fe(CO)^+$, $(P_3^{Si})Fe(CNMe)^+$, and $(P_3^{Si})Fe(N_2)^+$, are: δ = 0.31 mm s^{-1}, ΔE_Q = 4.12 mm s^{-1} ; δ = 0.41 mm s^{-1}, ΔE_Q = 3.14 mm s^{-1}; δ = 0.53 mm s^{-1}, ΔE_Q = 2.39 mm s^{-1} respectively.
53. Tao, J.; Perdew, J. P.; Staroverov, V. N.; Scuseria, G. E. *Phys. Rev. Lett.* **2003**. 91, 146401–146404.
54. Weigend, F. *Phys. Chem. Chem. Phys.* **2006**. 8, 1057–1065.
55. Matson, B. D.; Peters, J. C. *ACS Catal.* **2018**. 8, 1448–1455.
56. As an example, explicit solvent interactions are often required to accurately predict reduction potentials, as recently observed for persulfate oxidation: Hosseini, S.; Janusz, J. N.; Tanwar, M.; Pendergast, A. D.; Neurock, M.; White, H. S. *J. Am. Chem. Soc.* **2022**. 144, 21103–21115.
57. Jolly, P. W.; Pettit, R. *J. Am. Chem. Soc.* **1966**. 88, 5044–5045.
58. Brookhart, M.; Tucker, J. R.; Flood, T. C.; Jensen, J. *J. Am. Chem. Soc.* **1980**. 102, 1203–1205.
59. Aghazada, S.; Munz, D.; Heinemann, F. W.; Scheurer, A.; Meyer, K. *J. Am. Chem. Soc.* **2021**. 143, 17219–17225.
60. Lee, Y.; Mankad, N. P.; Peters, J. C. *Nat. Chem.* **2010**. 2, 558–565.
61. Mankad, N. P.; Whited, M. T.; Peters, J. C. *Angew. Chem. Int. Ed.* **2007**. 46, 5768–5771.
62. Benson, S. W. *J. Chem. Educ.* **1965**. 42, 502.
63. Attempts to optimize $[Fe{=}C(H)NH_3]^0$ showed *in silico* C−N bond cleavage; the energy of this intermediate was hence estimated by constrained geometry optimization with the C−N bond set to 1.6 Å.

64. Suess, D. L. M.; Peters, J. C. *J. Am. Chem. Soc.* **2013**. 135, 12580–12583.

65. Wang, Y.; Silva, J. J. R. F. D.; L. Pombeiro, A. J.; Angela Pellinghelli, M.; Tiripicchio, A.; A. Henderson, R.; L. Richards, R. *J. Chem. Soc. Dalton Trans.* **1995**. 7, 1183–1191.

66. Filippou, A. C.; Grünleitner, W.; Völkl, C.; Kiprof, P. *Angew. Chem. Int. Ed. Engl.* **1991**. 30, 1167–1169.

67. Filippou, A. C.; Völkl, C.; Grünleitner, W.; Kiprof, P. *J. Organomet. Chem.* **1992**. 434, 201–223.

68. The overaddition of CN^- ligand was not observed in the reaction of (P_3^{Si})FeOTf and [TBA][CN]. Similarly, (P_3^{Si})FeCN is synthesized with excess NaCN in refluxing 1:1 THF:MeOH, but addition of multiple equivalents of CN^- has not been observed.

69. Turculet, L.; Feldman, J. D.; Tilley, T. D. *Organometallics* **2003**. 22, 4627–4629.

70. Hill, P. J.; Doyle, L. R.; Crawford, A. D.; Myers, W. K.; Ashley, A. E. *J. Am. Chem. Soc.* **2016**. 138, 13521–13524.

71. Yandulov, D. V.; Schrock, R. R. *Inorg. Chem.* **2005**. 44, 1103–1117.

72. Thimm, W.; Gradert, C.; Broda, H.; Wennmohs, F.; Neese, F.; Tuczek, F. *Inorg. Chem.* **2015**. 54, 9248–9255.